Metals **2015**, *5*, 216-227; doi:10.3390/met5010216

OPEN ACCESS

metals

ISSN 2075-4701

www.mdpi.com/journal/metals/

Article

Hot Deformation Behavior of Ti-3.5Al-5Mo-6V-3Cr-2Sn-0.5Fe Alloy in α + β Field

Zhaoxin Du [1,*], Shulong Xiao [2], Jingshun Liu [1], Shufeng Lv [1], Lijuan Xu [2], Fantao Kong [2] and Yuyong Chen [2]

[1] School of Materials Science and Engineering, Inner Mongolia University of Technology, Hohhot 010051, China; E-Mails: Jingshun_Liu@163.com (J.L.); shufenglu@yahoo.com (S.L.)

[2] National Key Laboratory of Science and Technology on Precision Heat Processing of Metals, Harbin Institute of Technology, Harbin 150001, China; E-Mails: xiaoshulong@hit.edu.cn (S.X.); xljuan@hit.edu.cn (L.X.); kft@hit.edu.cn (F.K.); yychen@hit.edu.cn (Y.C.)

***** Author to whom correspondence should be addressed; E-Mail: duzhaoxin@163.com; Tel.: +86-471-65757532.

Academic Editor: M. T. Whittaker

Received: 10 January 2015 / Accepted: 3 February 2015 / Published: 13 February 2015

Abstract: The deformation behavior of Ti-3.5Al-5Mo-6V-3Cr-2Sn-0.5Fe high strength β titanium alloy is systematically investigated by isothermal compression in α + β field with the deformation temperatures ranging from 1003 K to 1078 K, the strain rates ranging from 0.001 s^{-1} to 1 s^{-1} and the height reduction is around 50%. Essentially, the flow stress-strain curve of isothermal compression in α + β field exhibits a flow softening feature when the strain rate is higher than 0.1 s^{-1} as while it exhibits a steady-state feature as the strain rate is lower than 0.1 s^{-1}. The peak stress increases with a decrease in deformation temperature and the increase of strain rate. The activation energy for deformation in α + β field was calculated and the average activation energy of 271.1 kJ/mol. The microstructure observation reveals that the isothermal deformation in the α + β field of the alloy is mainly controlled by the dynamic recovery mechanism accompanied with the secondary dynamic recrystallizitation of β phase. The α phase shows an obvious pinning effect for the movement of dislocations. During deformation, the α phase was elongated and fragmented.

Keywords: β titanium alloys; activation energy; microstructure evolution; deformation mechanism

1. Introduction

Generally, β titanium alloys possess the wide applied range in the applications of aerospace industries due to their excellent mechanical properties [1–3]. The mechanical properties of β titanium alloys are mainly controlled by microstructure, especially the grain size, volume fraction and morphology of α phase (primary, secondary and grain boundary α) [4–7]. For example, Terlinde *et al.* [4] have proven that the Ti-10V-2Fe-3Al with globular α microstructure shows better ductility than elongated α microstructure. However, the disadvantage of β titanium alloys is the poor ductility in high strength level, such as Timetal555 alloy [8]. Fortunately, the mechanical properties of β titanium alloys can be optimized through effectively microstructural controlling during the different stages of thermomechanical processing [9]. Usually, β titanium alloys are forged in the β field to break down the coarse grain microstructure, and then finally forged at the β or α + β field. It should be pointed out that the desired properties of titanium alloys are dependent on the final thermomechanical processing [10–12]. Studies done by Srinivasu *et al.* [13] have proved that rolling Ti-10V-2Fe-3Al alloy in α + β field exhibited better ductility than rolling in β field. Thus, the minimal α + β forging should be carried out if a good ductility is required.

Many works have been conducted on α + β titanium alloys through isothermal compression method to understand deformation mechanisms and microstructure controlling, the majority of these works are mainly focused on the Ti-6Al-4V alloy [14–19]. It is well known that the main deformation mechanism for deformation in β field is dynamic recovery of β titanium alloys, while it is also difficult to determine the deformation mechanism for deformation in α + β field owing to the complex microstructure parameters. Typically, the microstructure of α + β processed β titanium alloys consists of a small sized of α phase, which is a vital factor affecting the flow behavior. There are few works has been done aobut β titanium alloys deformation in α + β field [20–23]. During the deformation of β titanium alloys in α + β field, the α phase could act as a harder particle to pinning the dislocation movement [23] and results in a higher peak stress. Material with high aspect ratio Widmanstätten α platelets produces higher flow stresses than material with globular primary α in subtransus deformation [24]. The flow stress increases with the increasing of volume fraction of α phase at certain strain rate [20]. Technically, the volume fraction of α phase is mainly controlled by deformation temperature, and the strain has little effect on the volume fraction of α phase at the temperatures investigated [25].

Ti-3.5Al-5Mo-6V-3Cr-2Sn-0.5Fe alloy is a newly developed β high strength titanium alloy. The previous work has shown that the alloy exhibits the excellent mechanical property with finally forging in the α + β field and followed by heat treatment [26]. The isothermal compression study has not carried on this alloy yet. This paper aims to investigate the flow behavior and microstructural evolution during isothermal compression in α + β field to accurately determine the hot working process of Ti-3.5Al-5Mo-6V-3Cr-2Sn-0.5Fe alloy.

2. Materials and Methods

The investigations were conducted on Ti-3.5Al-5Mo-6V-3Cr-2Sn-0.5Fe high strength β titanium alloy. The alloy was melted using double vacuum consumable arc melting process to obtain an original ingot. The ingot was pre-forged in the α + β field to a round bars with the diameter of 80 mm. The β transition

temperature of the alloy measured by metallographic method is about 1088 K. The microstructure of pre-forged alloy is shown in Figure 1, the α phase showed equiaxed shape and some β subgrains with small size formed in the matrix. The cylindrical specimens with 8.0 mm in diameter and 12.0 mm in height were machined from the pre-forged Ti-3.5Al-5Mo-6V-3Cr-2Sn-0.5Fe alloy bar. The isothermal compression experiment was conducted on a Gleeble-1500dD simulator (Dynamic Systems Inc., Poestenkill, NY, USA) at the deformation temperatures ranging from 1003 K to 1078 K with an interval of 25 K, the strain rates of 0.001 s^{-1}, 0.01 s^{-1}, 0.1 s^{-1}, 1 s^{-1} respectively and the height reduction of 50%. The specimens were heated to compression temperature at a heating rate of 15 Ks^{-1} and held for 3 min before compression. After hot compression, the specimens were cooled in air to room temperature. Microstructure observation of the alloy was characterized by scanning electron microscopy (SEM) and electron backscattered diffraction (EBSD) by using field emission gun scanning electron microscopy Quanta 200FEG (FEI company, Hillsboro, OR, USA). The specimens for SEM and EBSD analysis were roughly polished with 400–2000 grid SiC paper in water, and then electropolished for 150 s at 1 V in reagent of 60% methanol, 30% butyl alcohol and 10% perchlorate at room temperature. The specimens for SEM observation were etched in the Kroll's reagent (Tianjin Yongda Chemical Reagent Co., Ltd., Tianjing, China) (mixed with 10 mL HF, 30 mL HNO_3 and 200 mL H_2O).

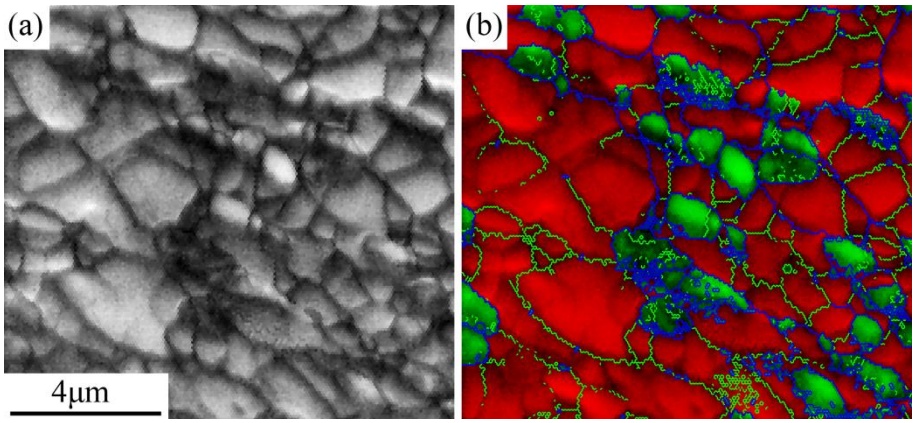

Figure 1. Microstructure of the alloy as-received: (**a**) image quality map; (**b**) grain boundary distribution plus phase map. The red field = β phase, green field = α phase, blue line = high angle grain boundaries (HAGBs, $\theta \geq 15°$), green line = low angle grain boundaries (LAGBs, $15° \geq \theta \geq 2°$).

3. Results and Discussion

3.1. Flow Stress Behavior

The true stress-strain curves of isothermally compressed deformation of Ti-3.5Al-5Mo-6V-3Cr-2Sn-0.5Fe alloy at different temperatures and strain rates are shown in Figure 2. It can be seen that the flow stress increases sharply with increasing of strain at the beginning stage of deformation. It is just the result of the work hardening behavior resulting from the increasing of dislocation density in the initial stages of deformation. The curves exhibit the steady state flow after an initial sharp peak, except the curves at strain rate of 1 s^{-1} which exhibit dynamic obvious softening behavior. At strain rate of 1 s^{-1} and temperatures of 1003 K, the curve exhibits an increase in true stress after a broad softening, this may be

due to the faster dislocation multiplication than dislocation motion resulting from high strain rate and low temperature. It is difficult to determine the deformation mechanisms only according to the shape of the true stress-true strain curves because that the flow softening behavior can be resulted from several reasons, such as dynamic recrystallization, temperature rise of the specimen and texture evolution, or grain size increase during the deformation process [27]. The characteristic of the flow stress tends to a steady value, it is caused by a combination of work hardening and dynamic softening mechanism. After the flow stress reaches the peak value, the effect of work hardening and softening comes to dynamic equilibrium and the flow stress ends to be a steady value.

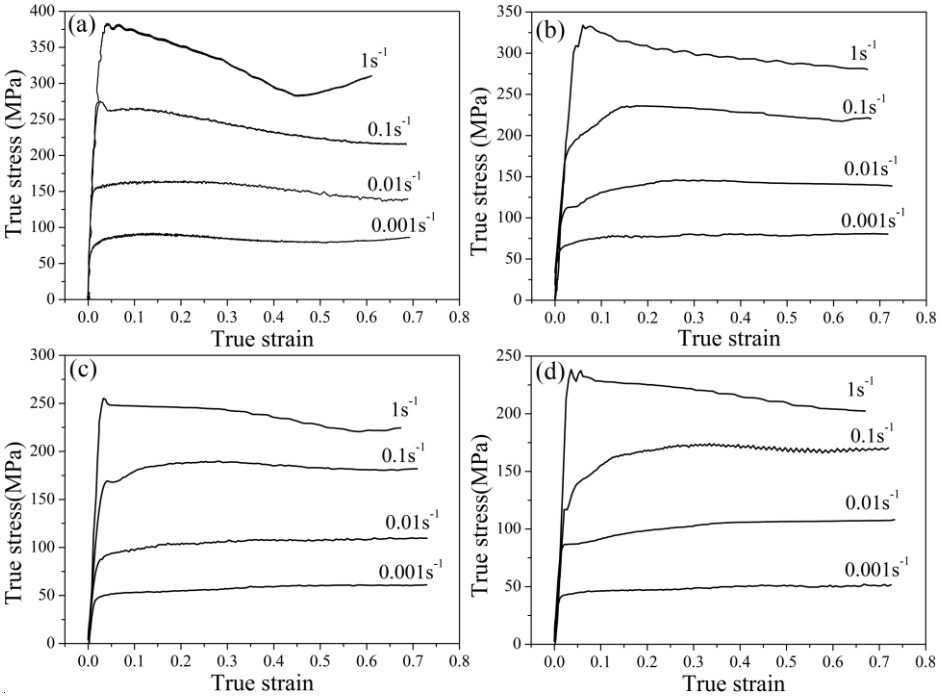

Figure 2. Compressive true stress- strain curves of the alloy under different temperature as follows: (**a**) 1003 K; (**b**) 1028 K; (**c**) 1053 K; (**d**) 1078 K.

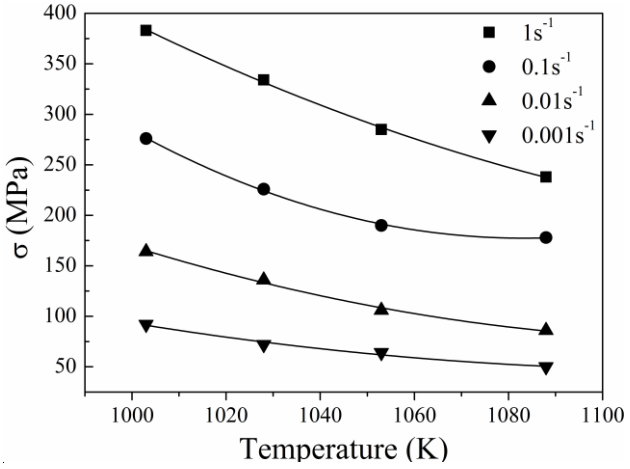

Figure 3. Effect of deformation temperature and strain rate on the peak flow stress.

Figure 3 shows the effects of deformation temperature and strain rate on the peak flow stress in isothermal compression of Ti-3.5Al-5Mo-6V-3Cr-2Sn-0.5Fe alloy. It can be seen that the peak flow

stress is so sensitive to the deformation temperature and strain rate. The peak stress increases with the decreasing of deformation temperature and increasing of strain rate. Such as that at a strain rate of 1 s^{-1}, the peak flow stress at 1003 K is higher by about 145 MPa than at a temperature of 1078 K. Moreover, the peak flow stress at strain rate of 1 s^{-1} is higher by about 295 MPa than at strain rate of 0.001 s^{-1} at a same deformation temperature of 1003 K. During the deformation of β titanium alloy in α + β field, the α phase could play a role of a harder particle dispersed in the soft matrix pinning the dislocation movement [23]. However, the volume fraction of α phase decreases with the increasing of deformation temperature. It also leads to a reduction of obstacles for dislocation moving and thus resulted in decrease of flow stress. Oppositely, the high volume fraction of α phase will lead to higher flow stress. There is a support for this position from other studies [20]. In addition, the lower strain rate provides more time to climp and be consumed of the dislocations and with the result that the flow stress increases with the increasing of strain rate.

3.2. Activation Energy

Based on the true flow stress-true strain data from compression test, the Arrhenius type equation which is proposed by Sellars *et al.*, is employed to establish the constitutive equation for alloy and designated as Equation (1) [28]:

$$\dot{\varepsilon}=A\left[\sin h\left(\alpha\sigma\right)\right]^{n}\exp\left[-Q/RT\right] \tag{1}$$

where $\dot{\varepsilon}$ is strain rate, A, α, n are constants independent of temperature, Q is activation energy, R is gas constant (R = 8.3145 J ‧mol^{-1} ‧k^{-1}), T is the absolute temperature.

The Equation (1) shows different expressions for different (ασ) values as follows:

$$\dot{\varepsilon}=A_1\sigma^{n_1} \qquad \alpha\sigma<0.8 \tag{2}$$

$$\dot{\varepsilon}=A_2\exp\left(\beta\sigma\right) \qquad \alpha\sigma>1.2 \tag{3}$$

Assuming that the deformation activation energy Q has no correlation to do with the deformation temperature of T, and the taking logarithm of both sides of Equations (1)–(3), the following equations can be obtained by:

$$\frac{\partial(\ln\dot{\varepsilon})}{\partial\{\ln[\sin h(\alpha\sigma)]\}}\Big|_{1/T}=n \tag{4}$$

$$\frac{\partial(\ln\dot{\varepsilon})}{\partial(\ln\sigma)}\Big|_{1/T}=n_1 \tag{5}$$

$$\frac{\partial(\ln\dot{\varepsilon})}{\partial\sigma}\Big|_{1/T}=\beta \tag{6}$$

The α can then be calculated based on the values of β and n_1, β = αn1. The material constant α is calculated and the obtained value is 0.00639. The activation energy of Q can be deduced from Equation (1):

$$Q=Rn\{\frac{\partial\ln[\sin h(\alpha\sigma)]}{\partial(1/T)}\}\Big|_{\dot{\varepsilon}}=R\frac{\partial\ln\dot{\varepsilon}}{\partial\ln[\sin h(\alpha\sigma)]}\Big|_{1/T}\cdot\left\{\frac{\partial\ln[\sin h(\alpha\sigma)]}{\partial(1/T)}\right\}\Big|_{\dot{\varepsilon}} \tag{7}$$

The calculated values of Q are 285.7 kJ/mol (1003 K), 283.33 kJ/mol (1028 K), 261 kJ/mol (1053 K), 254.4 kJ/mol (1078 K) respectively. The activation energy represents the energy level to overcome in some atomistic mechanisms such as diffusion. In this study, the activation energy for deformation in α + β field decreased with the increasing of temperature. This is mainly caused by the decreasing of volume fraction of α phase. The average activation energy in α + β deformation field is 271.1 kJ/mol, it is quite similar to Ti-5Al-5Mo-5V-1Cr-1Fe β alloy (291.73 ± 50 kJ mol^{-1}) obtained by Liu [20] and Ti-5Al-5Mo-5V-3Cr-1Zr β alloy (275 $kJmol^{-1}$) obtained by Warchomicka *et al.* [23]. In titanium alloys, the activation energies for self-diffusion in α and β titanium have been reported as 183 kJ mol^{-1} and 153 $kJmol^{-1}$ respectively [29]. It is well known that the activation energy of deformation close to self-diffusion in the β phase suggesting that the deformation is practically dominated by dynamic recovery of β phase. However, the activation energy in present study is higher than self-diffusion of β phase. The reason for higher activation energy in α + β field is possibly resulted from the presence of α phase. McQueen [30] pointed out that the activation energy will rise due to additions of solute, precipitates, dispersoid, reinforcements and inclusions. In titanium alloys, Warchomicka [23] considered that the higher activation energy deformed in α + β field should be related to the energy necessary to rotate, elongate and the α grains. In addition, the α phase shows the pining effect on the dislocation movement as mentioned above. The more α phase resulting from lower temperature creates more obstacles and then the higher activation energy should be provided for dislocation movement. Therefore, a common ground can be deduced from as mentioned above that the presence of the α phase should be the reason for higher activation energy deformed in the α + β field rather than activation energy for self-diffusion of β phase.

3.3. Microstructure Observation

Figure 4 shows the microstructure of Ti-3.5Al-5Mo-6V-3Cr-2Sn-0.5Fe under different deformation temperatures with strain rate of 0.01 s^{-1}. The white area on the SEM image is α phase. The volume fraction of α phase decreased with the increase of deformation temperature, as can be seen from Figure 4. At a lower deformation temperature of 1003 K, the α phase showed three kinds of shape, namely equiaxed α, lamellar α with smaller size and the elongated α with larger size. The smaller α lamellar phase disappeared at temperature 1028 K, and the elongated α phase disappeared up to 1078 K. The volume fraction of equaixed α phase decreased with an increase of temperature, but the size almost is no change at all deformation temperatures. The dynamic recovery phenomenon of α phase can be observed in the present study. It can be observed that some equiaxed α grains exist between elongated α phases in Figure 4a. This suggesting a mechanism of fragmentation of elongated α phases. Margolin and Cohen proposed a model for the globularisation of α phase and the mechanism can be summarized as follows [31,32]. Initially, the recrystallised α grains are formed within the α plate. While the 180° dihedral angle between the α/α boundary can not exist due to the surface tension requirement. Thus, a driving force is provided for the movement of some beta phase into the α/β boundaries and simultaneous rotation of the of the α/β boundaries. Subsequent working will separate the neighbouring recrystallizated α phases and leads to equiaxed shape of the α phases. The mechanism of fragmentation of α phases is not only good applicable to the deformation of α + β titanium alloys with lamellar microstructure [17,31,33,34], but also to β titanium alloys [13,24].

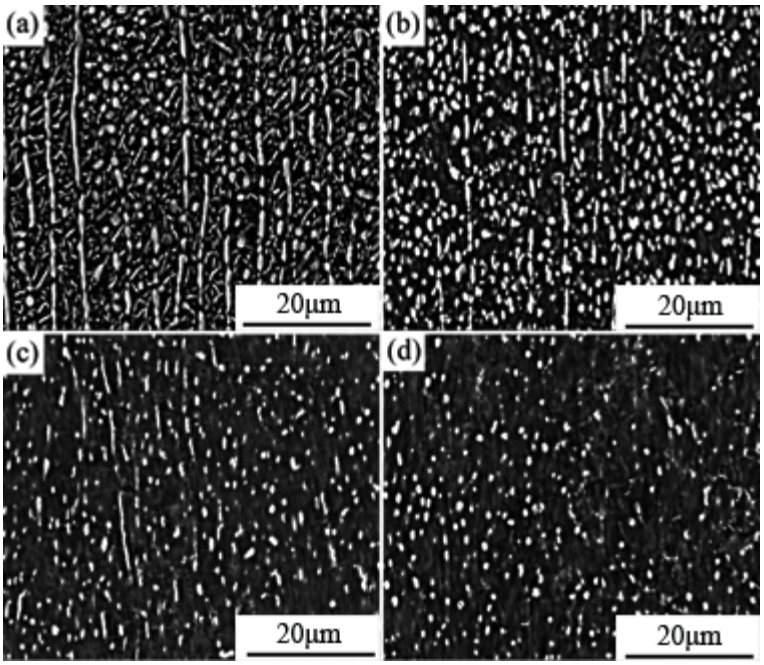

Figure 4. Morphology of the alloy deformed at different temperatures with strain rate of 0.01 s^{-1}: (**a**) 1003 K; (**b**) 1028 K; (**c**) 1053 K; (**d**) 1078 K.

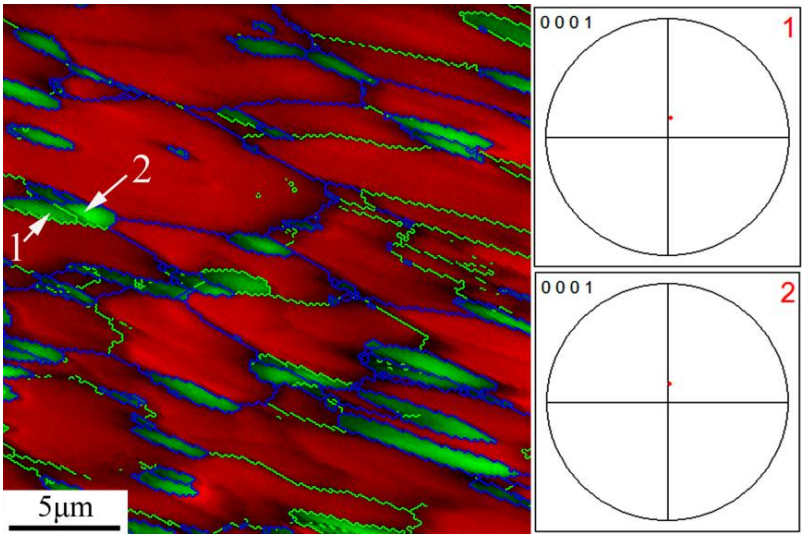

Figure 5. Phase composition and grain boundary map of the alloy deformed at 1028 K with the strain rate of 0.001 s^{-1}. (The red field = β phase, green field = α phase, blue line = HAGBs ($\theta \geq 15°$), green line = LAGBs ($15° \geq \theta \geq 2$ °).

The direct evidence for fragment of α phase displays in Figure 5. Figure 5 shows phase composition and grain boundary map of the alloy deformed at 1028 K with the strain rate of 0.001 s^{-1}. It is obvious that the α phase was also deformed during isothermal compression and elongated perpendicular to the compression direction. As indicated by white uni-directional arrows in Figure 5, a subboundary with low angle developed inside α phase, and the right panels of Figure 5 shows that each part of this α grain exhibits the same orientation. It can confirms that the dynamic recovery phenomenon of the α phase. Subsequent compression deformation can provide a driving force for penetration of β phase along the α/α subboundaries and then resulting in equiaxed morphology α phase. However, the low angle grain

boundaries are mainly distributed in β grains. It indicates that the β phase is mainly deformed. As previouly work reported by Jones *et al.* [25] indicated that the majority of the flow occurs within the β phase, but little load transfers to the α phase. The α phase plays a vital role of hindering effect of dislocation climp during hot processing in α + β field, taht it could act as a harder particle dispersed in the soft matrix pinning the dislocation movement and hence the β subgrains cannot grow beyond the α grains [23]. As shown in Figure 6, the α grains are mainly distributed in grain or subgrain boundary triple points, and the low angle grain boundaries terminated at α phase.

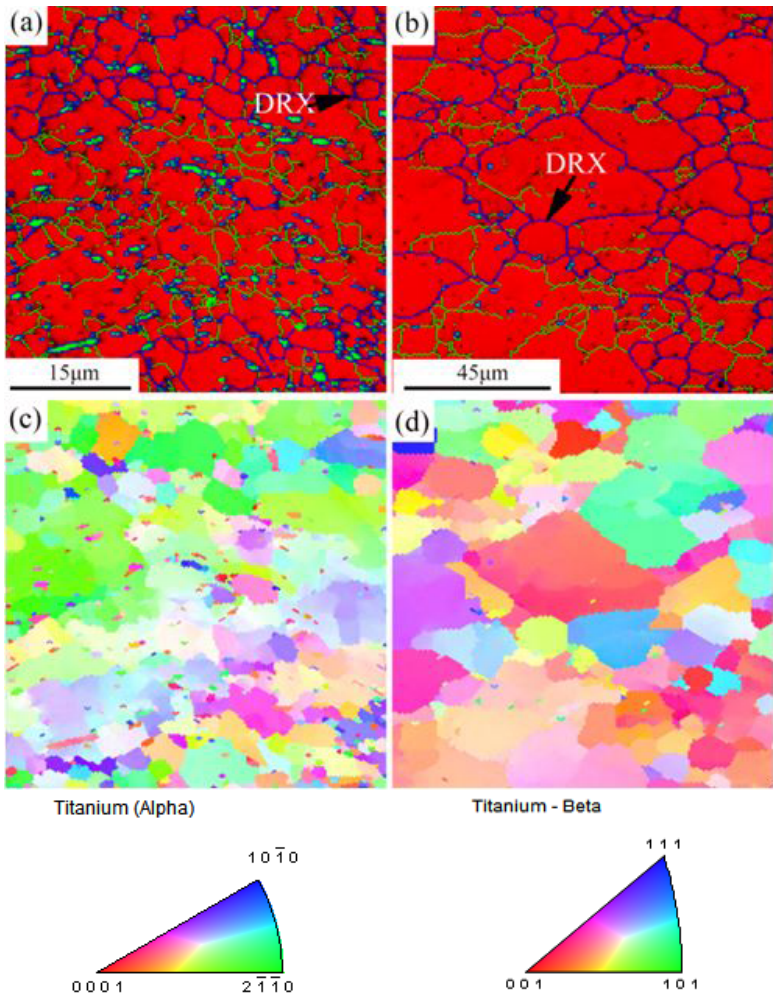

Figure 6. Electron backscattered diffraction (EBSD) images showing microstructure of the alloy deformed at 1003 K (**a**) and (**c**) 1078 K (**b**) and (**d**) with the strain rate of 0.001 s^{-1}. (In **a** and **b**), the red field = β phase, green field = α phase, blue line = HAGBs, green line = LAGBs, DRX = dynamic recrystallization).

Figure 6 shows the EBSD images of the alloy deformed at 1003 K and 1078 K with strain rate of 0.001 s^{-1}, respectively. The grain size deformated at 1003 K is quite smaller than high deformation temperature of 1078 K as can be seen from Figure 6a,b. The smaller grain size is attributed to the volume fraction of α phase. As mentioned above, the α phase acts as a harder particle dispersed in the soft matrix to pinning the moving dislocation and hence the β subgrains cannot grow beyond the α grains. Therefore, the more content of α phase obtained at lower deformation temperature resulting in small β grain or subgrain size. Some new formed equaixed β grains with large angle grain boundaries can be observed in

Figure 6a,b. However, most of the β grains with large angle grain boundaries in Figure 6a exhibit similar color with neighbor grains, as shown in inverse pole figure map as shown in Figure 6c. It means that these new β grains are obtained by rotation and growth of subgrains, and it can be conclued that the dynamic recovery is the dominant mechanism during deformation at lower temperature since there are also few in number of dynamic recrystallized β grains deformated at 1003 K. The dynamic recovery still is the dominant mechanism at higher deformation temperature of 1078 K, but the dynamic recrystallized β grains are more and larger than lower deformation temperature of 1003 K.

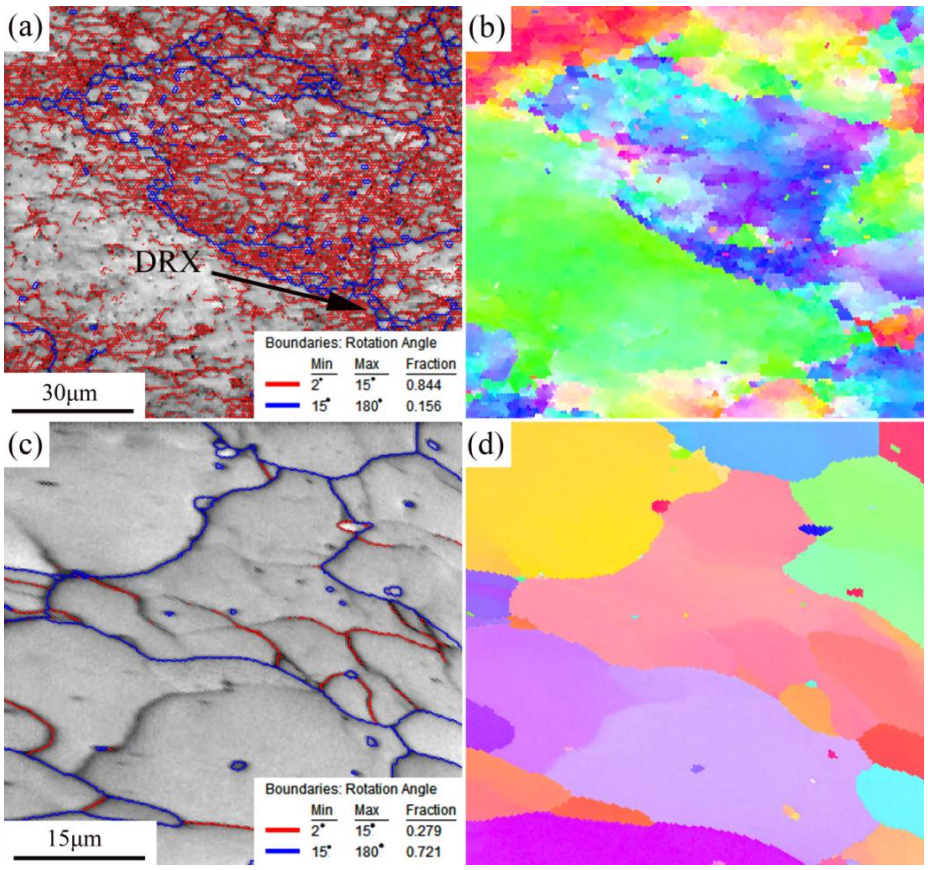

Figure 7. Grain boundary maps and inverse pole figure maps of the alloy deformed at 1078 K with the strain rate of 1 s^{-1} (**a**), (**b**) and 0.001 s^{-1} (In **a** and **c**), blue line = HAGBs, green line = LAGBs, DRX = dynamic recrystallization).

Figure 7 reveals the EBSD imaged of the alloy deformed at 1078 K with the strain rate of 1 s^{-1} and 0.001 s^{-1}. The microstructure of the alloy is very sensitive to the deformation strain rate. The higher strain rate of 1 s^{-1} resulted in large number fraction of low angle grain boundaries (Figure 7a) and formation of lots of sub-structures with small misorientation inside β grains (Figure 7b). However, at lower deformation strain rate of 0.001 s^{-1} the number fraction of low angle grain boundaries is much less than the high strain rate of 1 s^{-1} (compared with Figure 7a,c), and the sub-structures show larger size and less number (compared with Figure 7b,d). The alloy deformated at 1078 K and strain rate of 1 s^{-1} shows a serrated grain boundary, while the uniform grain boundary is obtained at the strain rate of 0.001 s^{-1}. The serrated grain boundary in large strain rate conditon caused by the existence of some new fine recrystallized β grains with high angle boundaries in the vicinity of boundaries as shown in Figure 7a (black arrow), but there is no appearance at the lower strain rate of 0.001 s^{-1}. The recrystallized

β grains are usually observed at the borders of β grains [35]. The content of low and high angle boundaries is relevant to deformation time. A massive dislocations produced during the process of isothermal deformation, but it seems no sufficient time to climp and be consumed because the high strain rate, and then reuslted in lots of number low angle grain boundaries inside β grains. On the contrary, the dislocations have sufficient time to climp and be consumed at lower strain rate conditions. Meanwhile, the recrystallized grains can also have more time to nucleation and growth at lowe strain rate. The evidence can be represented by comparision of Figures 6b and 7b, the recrystallized grains with lower strain rate shows a larger size than higher strain rate conditions.

4. Conclusions

The flow behavior and microstructural evolution of Ti-3.5Al-5Mo-6V-3Cr-2Sn-0.5Fe alloy during isothermal compression in α + β field has been investigated. The following principal conclusions can be drawn from the present study:

(1) The flow stress–strain curves of Ti-3.5Al-5Mo-6V-3Cr-2Sn-0.5Fe alloy isothermally compressed in α + β field exhibit a flow softening feature as the strain rate is higher than 0.1 s^{-1} while it exhibits a steady-state feature as the strain rate is lower than 0.1 s^{-1}. The peak stress increases with the decrease of deformation temperature and an increase of strain rate.

(2) The activation energy of Ti-3.5Al-5Mo-6V-3Cr-2Sn-0.5Fe alloy for deformation in α + β field was calculated. The average activation energy in α + β field deformation is 271.1 kJ/mol, it is higher than that of self-diffusion of β phase resulting from presence of α phase.

(3) The α phase shows an obvious pinning effect for the movement of dislocations deformed at α + β field. The high volume fraction of α phase is responsible for higher flow stress at lower deformation temperature.

(4) The deforamtion mechanism of Ti-3.5Al-5Mo-6V-3Cr-2Sn-0.5Fe alloy in α + β field is mainly attributed to dynamic recovery accompanied with dynamic recrystallizitation of β phase, but the dynamic recovery is dominant.

Acknowledgments

J.S.L. acknowledges the support from Scientific Research Foundation of Inner Mongolia University of Technology under grant Nos. ZD201405.

Author Contributions

Zhaoxin Du, Shulong Xiao, Lijuan Xu, Fantao Kong and Yuyong Chen conceived and designed the experiments; Zhaoxin Du and Shulong Xiao performed the experiments; Zhaoxin Du and Shulong Xiao, Jingshun Liu and Shufeng Lv analyzed the date; Zhaoxin Du wrote the paper.

Conflicts of Interest

The authors declare no conflict of interest.

References

1. Boyer, R.R.; Briggs, R.D. The use of β titanium alloys in the aerospace industry. *J. Mater. Eng. Perform.* **2005**, *14*, 681–685.
2. Boyer, R.R. An overview on the use of titanium in the aerospace industry. *Mater. Sci. Eng. A* **1996**, *213*, 103–114.
3. Boyer, R.R. Titanium for aerospace Rationale and applications. *Adv. Perform. Mater.* **1995**, *2*, 349–368.
4. Terlinde, G.T.; Duerig, T.W.; Williams, J.C. Microstructure, tensile deformation, and fracture in aged Ti-10V-2Fe-3Al. *Metall. Trans. A* **1983**, *14A*, 2101–2115.
5. Bhattacharjee, A.; Varma, V.K.; Kamat, S.V.; Gogia, A.K.; Bhargava, S. Influence of β grain size on tensile behavior and ductile fracture toughness of titanium alloy Ti-10V-2Fe-3Al. *Metall. Trans. A* **2006**, *37*, 1423–1433.
6. Ghosh, A.; Sivaprasad, S.; Bhattacharjee, A.; Kar, S.K. Microstructure-fracture toughness correlation in an aircraft structural component alloy Ti-5Al-5V-5Mo-3Cr. *Mater. Sci. Eng. A* **2013**, *568*, 61–67.
7. Kar, S.K.; Suman, S.; Shivaprasad, S.; Chaudhuri, A.; Bhattacharjee, A. Processing-microstructure-yield strength correlation in a near β Ti alloy, Ti-5Al-5Mo-5V-3Cr. *Mater. Sci. Eng. A* **2014**, *610*, 171–180.
8. Nyakana, S.; Fanning, J.; Boyer, R.R. Quick reference guide for β titanium alloys in the 00 s. *J. Mater. Eng. Perform.* **2005**, *14*, 799–811.
9. Weiss, I.; Semiatin, S.L. Thermomechanical processing of beta titanium alloys—An overview. *Mater. Sci. Eng. A* **1998**, *243*, 46–65.
10. Boyer, R.R. Design properties of a high-strength titanium alloy, Ti-10V-2F-3Al. *JOM* **1980**, *32*, 61–65.
11. Chen, C.C.; Boyer, R.R. Practical considerations for manufacturing high strength Ti-10V-2Fe-3Al forgings. *JOM* **1979**, *31*, 33–39.
12. Jones, N.G.; Jackson, M. On mechanism of flow softening in Ti-5Al-5Mo-5V-3Cr. *Mater. Sci. Technol.* **2011**, *27*, 1025–1032.
13. Srinivasu, G.; Natraj, Y.; Bhattacharjee, A.; Nandy, T.K.; Nageswara Rao, G.V.S. Tensile and fracture toughness of high strength β Titanium alloy, Ti-10V-2Fe-3Al, as a function of rolling and solution treatment temperatures. *Mater. Des*. **2013**, *47*, 323–330.
14. Zong, Y.Y.; Shan, D.B.; Xu, M.; Lv, Y. Flow softening and microstructural evolution of TC11 titanium alloy during hot deformation. *J. Mater. Process. Technol.* **2009**, *209*, 1988–1994.
15. Li, H.; Li, M.Q.; Han, T.; Liu, H.B. The deformation behavior of isothermally compressed Ti-17 titanium alloy in alpha plus beta field. *Mater. Sci. Eng. A* **2012**, *546*, 40–45.
16. Quan, G.Z.; Luo, G.C.; Liang, J.T.; Wu, D.S.; Mao, A.; Liu, Q. Modelling for the dynamic recrystallization evolution of Ti-6Al-4V alloy in two-phase temperature range and a wide strain rate range. *Comput. Mater. Sci.* **2015**, *97*, 136–147.
17. Zherebtsov, S.; Murzinova, M.; Salishchev, G.; Semiatin, S.L. Spheroidization of the lamellar microstructure in Ti-6Al-4V alloy during warm deformation and annealing. *Acta Mater.* **2011**, *59*, 4138–4150.

18. Zhao, J.; Ding, H.; Zhao, W.; Jiang, Z. Effects of hydrogen on the hot deformation behaviour of Ti-6Al-4V alloy: Experimental and constitutive model studies. *J. Alloy. Compd.* **2013**, *574*, 407–414.
19. Kim, J.H.; Semiatin, S.L.; Lee, C.S. Constitutive analysis of the high-temperature deformation mechanisms of Ti-6Al-4V and Ti-6.85Al-1.6V alloys. *Mater. Sci. Eng. A* **2005**, *394*, 366–375.
20. Liu, S.F.; Li, M.Q.; Luo, J.; Yang, Z. Deformation behavior in the isothermal compression of Ti-5Al-5Mo-5V-1Cr-1Fe alloy. *Mater. Sci. Eng. A* **2014**, *589*, 15–22.
21. Liang, H.; Guo, H.; Ning, Y.; Peng, X.; Qin, C.; Shi, Z. Dynamic recrystallization behavior of Ti-5Al-5Mo-5V-1Cr-1Fe alloy. *Mater. Des.* **2014**, *63*, 798–804.
22. Li, C.; Zhang, X.Y.; Zhou, K.C.; Peng, C.Q. Relationship between lamellar α evolution and flow behavior during isothermal deformation of Ti-5Al-5Mo-5V-1Cr-1Fe near β titanium alloy. *Mater. Sci. Eng. A* **2012**, *558*, 668–674.
23. Warchomicka, F.; Poletti, C.; Stockinger, M. Study of the hot deformation behaviour in Ti-5Al-5Mo-5V-3Cr-1Zr. *Mater. Sci. Eng. A* **2011**, *528*, 8277–8285.
24. Jackson, M.; Jones, N.G.; Dye, D.; Dashwood, R.J. Effect of initial microstructure on plastic flow behaviour during isothermal forging of Ti-10V-2Fe-3Al. *J. Mater. Sci. Eng. A* **2009**, *501*, 248–254.
25. Jones, N.G.; Dashwood, R.J.; Dye, D.; Jackson, M. Thermomechanical processing of Ti-5Al-5Mo-5V-3Cr. *Mater. Sci. Eng. A* **2008**, *490*, 369–377.
26. Du, Z.X.; Xiao, S.L.; Xu, L.J.; Tian, J.; Kong, F.T.; Chen, Y.Y. Effect of heat treatment on microstructure and mechanical properties of a new β high strength titanium alloy. *Mater. Des.* **2014**, *55*, 183–190.
27. Li, L.X.; Lou, Y.; Yang, L.B.; Peng, D.S.; Rao, K.P. Flow stress behavior and deformation characteristics of Ti-3Al-5V-5Mo compressed at elevated temperatures. *Mater. Des.* **2002**, *23*, 451–457.
28. Sellars, C.M.; McTegart, W.J. On the mechanism of hot deformation. *Acta Metall.* **1966**, *14*, 1136–1138.
29. Dyment, F.; Libanati, C.M. Self-diffusion of Ti, Zr, and Hf in their HCP phases, and diffusion of Nb95 in HCP Zr. *J. Mater. Sci.* **1968**, *3*, 349–359.
30. McQueen, H.J.; Ryan, N.D. Constitutive analysis in hot working. *Mater. Sci. Eng. A* **2002**, *322*, 43–63.
31. Margolin, H.; Cohen, P. Evolution of the equiaxed morphology of phases in Ti-6Al-4V. In *Titanium 80: Science and Technology*; Warrendale, TMS-AIME: Kyoto, Japan, 1980; pp. 1555–1561.
32. Margolin, H.; Cohen, P. Kinetics of Evolution of Alpha in Ti-6Al-4V. In *Titanium 80: Science and Technology*; Warrendale, TMS-AIME: Kyoto, Japan, 1980; pp. 2991–2997.
33. Wang, K.X.; Zeng, W.D.; Zhao, Y.Q.; Lai, Y.J.; Zhang, X.M.; Zhou, Y.G. Flow behaviour and microstructural evolution of Ti-17 alloy with lamellar microstructure during hot deformation in alpha plus beta phase field. *Mater. Sci. Technol.* **2011**, *27*, 21–28.
34. Weiss, I.; Froes, F.H.; Eylon, D.; Welsch, G.E. Modification of alpha morphology in Ti-6Al-4V by thermomechanical processing. *Metall. Trans. A* **1986**, *17A*, 1935–1947.
35. OuYang, D.L.; Fu, M.W.; Lu, S.Q. Study on the dynamic recrystallization behavior of Ti-alloy Ti-10V-2Fe–3Al in β processing via experiment and simulation. *Mater. Sci. Eng. A* **2014**, *619*, 26–34.